


Article

Diurnal Air Temperature Modeling Based on the Land Surface Temperature

Mehdi Gholamnia, Seyed Kazem Alavipanah *, Ali Darvishi Boloorani, Saeid Hamzeh and Majid Kiavarz 

Faculty of Geography, Department of Remote Sensing and GIS, University of Tehran, Tehran 1417466191, Iran; Mehdi_gholamnia@ut.ac.ir (M.G.); ali.darvishi@ut.ac.ir (A.D.B.); saeid.hamzeh@ut.ac.ir (S.H.); kiavarzmajid@ut.ac.ir (M.K.)

* Correspondence: salavipa@ut.ac.ir, Tel.: +98-21-6111-3536

Received: 27 July 2017; Accepted: 30 August 2017; Published: 1 September 2017

Abstract: The air temperature is an essential variable in many applications related to Earth science. Sporadic spatial distribution of weather stations causes a low spatial resolution of measured air temperatures. This study focused on modeling the air diurnal temperature cycle (DTC) based on the land surface temperature (LST) DTC. The air DTC model parameters were estimated from LST DTC model parameters by a regression analysis. Here, the LST obtained from the INSAT-3D geostationary satellite and the air temperature extracted from weather stations were used within the time frame of 4 March 2015 to 22 May 2017 across Iran. Constant parameters of the air DTC model for each weather station were estimated based on an experimental approach over the time period. Results showed these parameters decrease as elevation increases. The mean absolute error (MAE) and the root mean square error (RMSE) for three hours sampling were calculated. The MAE and RMSE ranges were between $[0.1, 4]$ °C and $[0.1, 3.3]$ °C, respectively. Additionally, 95% of MAEs and RMSEs were less than 2.9 °C and 2.4 °C values, correspondingly. The range of the mean values of MAEs and RMSEs for a three-hour sampling time were $[-0.29, 0.6]$ °C and $[2, 2.11]$ °C. The DTC model results showed a meaningful statistical fitting in both air DTCs modeled from LST and weather station-based DTCs. The variability of mean error and RMSE in different land covers and elevation classes were also investigated. In spite of the complex behavior of the environmental variables in the study area, the model error bar did not show significantly biased estimations for various classes. Therefore, the developed model was less sensitive to variations of land covers and elevation changes. It can be conclude that the coefficients of regression between LST and air DTC could model properly the environmental factors.

Keywords: air temperature; LST; DTC model; satellite; weather station

1. Introduction

Air temperature (T_a) is one of the main inputs in several models in hydrology, climate, meteorology, etc. [1–5]. Well-timed T_a measurements in weather stations are carried out worldwide. Such data are limited to point-based recording in ground stations with a sparse spatial distribution. Therefore, there is not an acceptable coverage of weather stations-based T_a measurements. Spatial interpolation is a method for achieving a geographical continuous data, but this method is strongly dependent on the density of weather stations and their spatial heterogeneity [6]. Remote sensing images with a synoptic coverage and proper temporal resolution can be considered as an alternative or complementary source for T_a measurements. Emphasizing on the unique characteristics of remotely sensed imagery, many studies have studied the relationship between satellite derived surface and air temperature. Geostationary and polar satellites are able to provide high temporal and spatial resolution data with nearly global coverage. The temporal patterns of

air temperature is complicated because it is influenced by a broad range of variable parameters, like wind speed, time, sky condition, solar zenith angle, soil moisture, location, albedo, emissivity, and thermal inertia [7]. Some of these parameters cannot be measured by remote sensing. Researchers are trying to develop methodologies to include the effects of these parameters in their modeling. Most of the developed methods are time- and location-dependent and are not applicable in other cases. According to Zakšek and Schroedter-Homscheidt [8], the developed methods are classified into three major categories: (1) Temperature–Vegetation Index (TVX) [9–12], which is based on the assumption that temperature of the vegetation canopy is almost equal to the ambient air temperature since their heat capacity is similar [7,9,10,13]. This method is sensitive to seasonality, soil moisture, and land cover type [14,15]; (2) The surface energy balance principle [6,7,16–18]. These approaches are based on net radiation, sensible heat flux, latent heat flux, and ground heat flux. Zhu et al. [19] mentioned that these models need many inputs which are not fully retrievable from remote sensing data; (3) Statistical approaches which recruit parametric and non-parametric machine learning approaches [14,16,18,20–30].

Such methods use ancillary data, such as Julian date, latitude, longitude, terrain, and vegetation indices to improve their modeling. Xu et al. [31] stated that linear regression cannot predict the air temperature based on LST in all conditions. They specified that Random Forest (RF) showed better accuracy than the multiple linear regression model. Air temperature modeling based on TVX and statistical methods are conducted based on discrete records of air temperatures in weather stations and the time between these records are not included in calculations. Furthermore, the effects of noise in recorded data caused by atmosphere forcing, cloud contamination, and other environmental conditions generate errors into the air temperature estimation. Diurnal modeling of LST and air temperature [32] can be beneficial in the modeling of T_a . Therefore, a synoptic coverage of T_a is obtainable. Jin and Dickinson [33] estimated the diurnal cycle of LST through temporal interpolation of NOAA-AVHRR. Sun et al. [34] used the same method for modeling Geostationary Operational Environmental Satellite (GOES) measurements. Alavipanah et al. [35] studied the application of LST DTC models for knowing the LST discrepancies between MODIS and geostationary satellites. Inamdar et al. [36] proposed an approach which employs MODIS imagery for calibration of GOES. They used both datasets to build half-hourly LSTs with 1 km spatial resolution. Stisen et al. [10] used TVX-based DTC modeling to acquire diurnal variation of air temperature. This research attempted to introduce methods that extract air temperature based on LST data by direct approach and without auxiliary environmental information. This study had three main goals: (1) estimating the LST DTC parameters in weather stations; (2) regression-driving of air temperature DTCs based on estimated parameters of LST DTCs; (3) comparing DTC parameters of LST and T_a ; and (4) evaluation of the modeled air DTC model by weather station observations.

2. The Study Area

Iran has an area of about 1648 million km² and is covered by mountain chains of Zagros from northwest to southwest. Alborz is in the north and several other topographic features surround the central plateau. Such heterogynous topographic conditions and geographical expansion of Iran create a variety of climate regions (Figure 1).

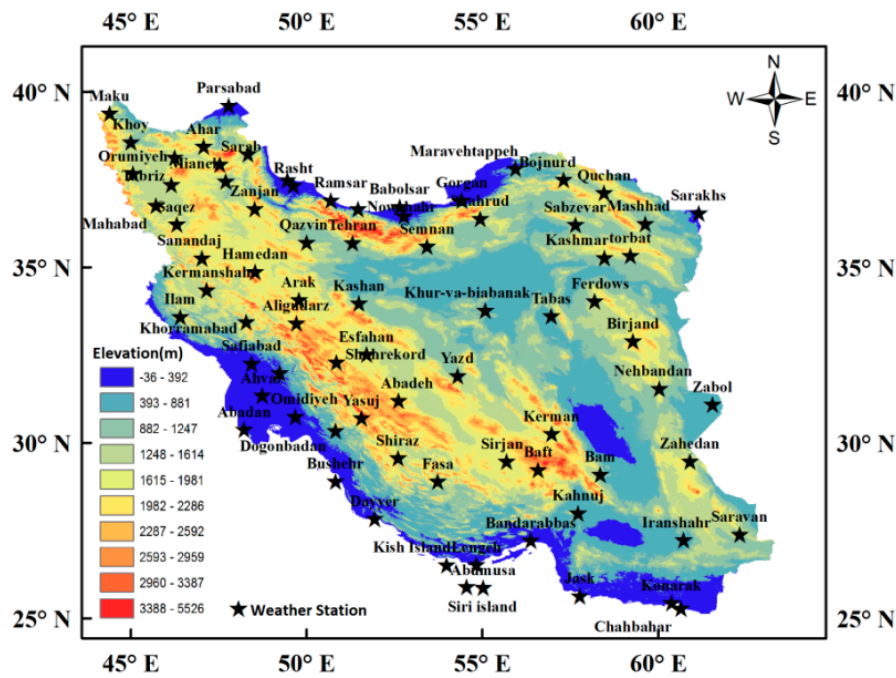


Figure 1. The study area and synoptic weather stations used to model air DTC.

3. Data

Satellite imagery: INSAT3-D is a geostationary satellite (82°E) launched on 26 July 2013 with Sounder and an Imager with six channels. LST product obtained from Imager images with half-hour temporal resolution by following equation [37]:

$$LST = b_0 + \left(b_1 + b_2 \frac{1 - \varepsilon}{\varepsilon} + b_3 \frac{\Delta \varepsilon}{\varepsilon^2} \right) \frac{T_i + T_j}{2} + \left(b_4 + b_5 \frac{1 - \varepsilon}{\varepsilon} + b_6 \frac{\Delta \varepsilon}{\varepsilon^2} \right) \frac{T_i - T_j}{2} + b_7 (T_i - T_j)^2 \quad (1)$$

where, b_i are coefficients and T_i is the brightness temperature at two thermal bands, i.e., i and j . ε is mean emissivity, $\varepsilon = \frac{\varepsilon_i + \varepsilon_j}{2}$, $\Delta \varepsilon$ is the emissivity difference, $\Delta \varepsilon = \varepsilon_i - \varepsilon_j$, derived from MODIS monthly emissivity products for two spectral bands i and j that are located at 11 μm and 12 μm . LST data from INSAT3-D-Imager was acquired from Meteorological and Oceanic Satellite Data Archival Centre (MOSDAC) in a time period from 4 March 2015 to 22 May 2017.

- Ground based weather data: T_a data from 77 weather stations with three-hour time intervals were obtained from 1 January 2000 to 22 March 2017 from I.R. of the Iran Meteorological Organization (IRIMO). Along with air temperature, sky condition, and wind speed data are also available.
- Elevation data: ASTER-DEM with 30 m spatial resolution was obtained from NASA Reverb website.
- Land cover map: Land cover type of the fifth category from MODIS land cover products with 500 m spatial resolution (MCD12Q1) was downloaded from NASA Reverb website.

4. Methodology

4.1. Air Temperature DTC Model

The developed DTC model for air temperature is based on [1,32] with some modifications under clear sky conditions for day and night using below equations:

$$T_{a\text{-day}}(t) = T_{\min} + (T_{\max} - T_{\min}) \cos\left(\frac{\pi}{\omega_{\text{air}}}(t - t_m)\right) \quad t < t_s \quad (2)$$

$$T_{a-nigh}(t) = T_{\min} + \left[(T_{\max} - T_{\min}) \cos\left(\frac{\pi}{\omega_{\text{air}}}(t_s - t_m)\right) \right] e^{\frac{(t-t_s)}{k}} \quad t > t_s \quad (3)$$

$$\omega_{\text{air}} = \omega + 2\beta \quad (4)$$

$$k = \frac{\omega_{\text{air}}}{\pi} \tan^{-1}\left(\frac{\pi}{\omega_{\text{air}}}(t_s - t_m)\right) \quad (5)$$

Day duration was calculated by using equation (6) introduced by [38]:

$$\omega = \frac{2}{15} \arccos(-\tan \varphi \tan \delta) \quad (6)$$

where φ is latitude and δ is solar declination which is related to DOY based on Equation (7) proposed by [39]:

$$\delta = 23.45 \sin\left(\frac{360}{365}(284 + \text{DOY})\right) \quad (7)$$

T_a is the air temperature at time t ; T_{\min} and T_{\max} are minimum and maximum diurnal air temperatures, respectively; t_m is time of maximum diurnal air temperature, t_s is the start time of air temperature free attenuation, ω is day duration, and ω_{air} is the width over the half period of the cosine term. β is the constant coefficients which was used to adapt the period of cosine term with air temperature variations. One should note that the time effect of β parameters is extended up to t_s and estimated as an experimental value which can be assumed constant. β values of 77 weather stations for those days were limited between 0 and 8 h with 0.1 intervals. Then, RMSE of DTC models for each day and each interval was calculated. Additionally, the mean of all RMSEs for each interval was calculated for the whole time series. The intervals with least RMSE were identified at each weather station and the corresponding values of β s were used for the DTC model construction. To estimate each DTC model free parameters, the Levenberg-Marquardt minimization scheme was applied [32,40].

4.2. LST DTC Model

The adapted DTC model in this study is based on GOT01_0 model proposed by Schädlich et al. [41]. The daily and nightly equations are as follows:

$$\text{LST}_d(t) = T_0 + A \cos\left(\frac{\pi}{\omega}(t - t_m)\right) \quad t < t_s \quad (8)$$

$$\text{LST}_n(t) = T_0 + \left[A \cos\left(\frac{\pi}{\omega}(t_s - t_m)\right) \right] e^{\frac{(t-t_s)}{k}} \quad t > t_s \quad (9)$$

$$k = \frac{\omega}{\pi} \tan^{-1}\left(\frac{\pi}{\omega}(t_s - t_m)\right) \quad (10)$$

As Figure 2 shows, T_0 is the residual temperature around sunrise (t_{sr}), A is the amplitude of LST, ω is day duration, t_m is the time of maximum diurnal LST, t_s is the starting point of free attenuation LST, K is the free attenuation coefficient. At least four observations are required to estimate T_0 , A , t_s , and t_m ; similar to the air DTC model, the Levenberg-Marquardt minimization scheme is used to estimate these free parameters.

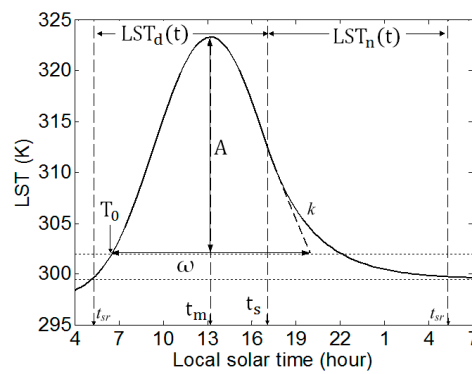


Figure 2. Got01_0 DTC model parameters [32].

4.3. T_a Construction from LST DTC

A regression modeling was used to estimate four free parameters of air DTC model (T_{\min} , T_{\max} , $t_{m_{\text{air}}}$, and $t_{s_{\text{air}}}$) based on LST DTC free parameters at each station for the whole dataset as follows (a_i and b_i are linear regression coefficients):

$$T_{\min} = a_1 + b_1 \times T_0 \quad (11)$$

$$T_{\max} = a_2 + b_2 \times (A + T_0) \quad (12)$$

$$t_{m_{\text{air}}} = a_3 + b_3 \times t_{m_{\text{LST}}} \quad (13)$$

$$t_{s_{\text{air}}} = a_4 + b_4 \times t_{s_{\text{LST}}} \quad (14)$$

In order to estimate the air DTC model, the LST data with reported clear sky days and homogeneous temporal distribution from 4 March 2015 to 22 May 2017 were used in the study area. LST DTC models of each weather stations were calculated and those DTC models with RMSEs less than and equal to 2 °C (approximately 85% of whole dataset) was selected for modeling. After that, 70% of the data were used for calibration of modeling in regression equations and the remained 30% was applied for evaluating the developed methodology. The mean absolute error (MAE) and the root mean square error (RMSE) were used to evaluate the results. The accuracy of air DTC modeling at each station was analyzed with respect to different elevation and land cover classes. The complete procedure for modeling air DTC is shown in Figure 3.

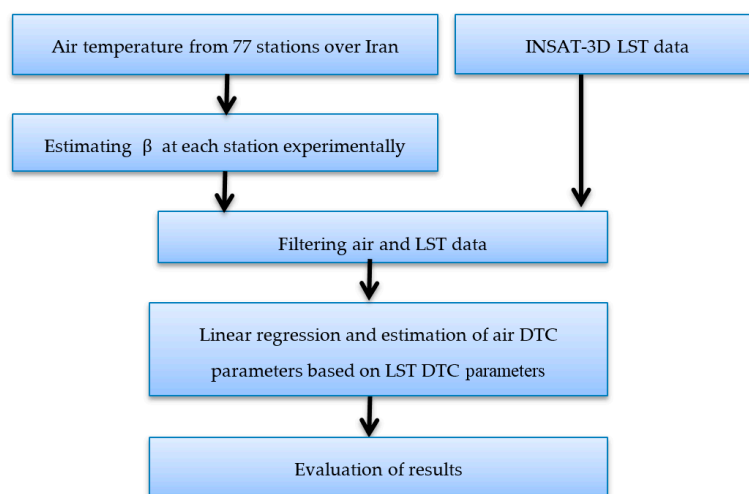


Figure 3. Flowchart of the proposed method to construct air DTC model from LST DTC parameters.

5. Results

To construct the air DTC model, estimation of β as a constant parameter was required. Estimation of this parameter was carried out experimentally. A range between zero and eight was considered for variation of β values over the whole time series and weather stations.

Figure 4a shows the air DTC model RMSEs with respect to β parameters for four sample weather stations (Abadan, Zabol, Ardebil, and Kish). Spatial variation of β for each weather station was depicted in Figure 4b. The value of β varied between three and eight, and in the south of Iran it had higher values. In order to construct the air DTC model, the data was filtered based on RMSEs of the LST DTC model. This caused a reduction in the number of weather stations to 54 for 4 March 2015 to 22 May 2017. Means and standard deviations (STD) of β values at weather stations for different elevations and land cover classes are shown in Figure 5. The highest elevation classes (1804 to 2252 m) with 2.94 mean and 0.34 STD values had lowest β range (Figure 5a). Grassland cover with 3.07 mean and 0.45 STD values had the lowest β (Figure 5b). The first elevation class (16 to 463 m) with 0.94 STD and shrub land cover with 1.05 STD had a maximum variation of β classes.

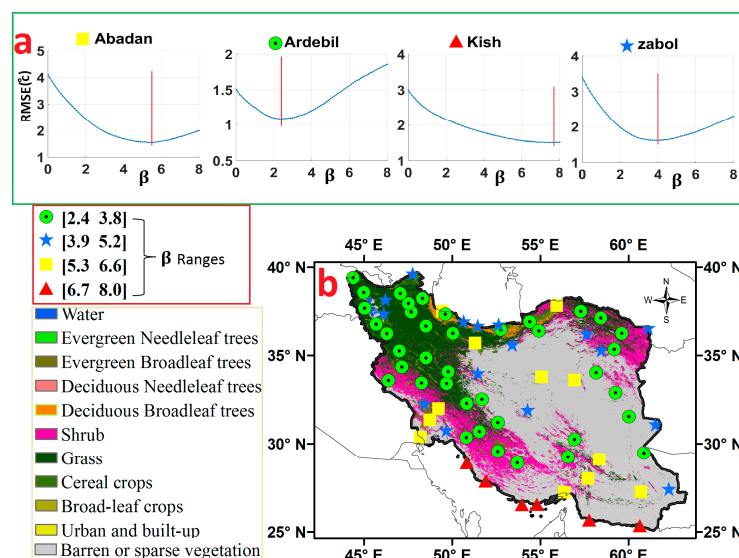


Figure 4. Estimated β range over study area for each weather station. (a) Empirical estimation of the β parameters for Abadan, Zabol, Ardebil, and Kish station, and (b) estimated β for all stations for different land covers in the study area.

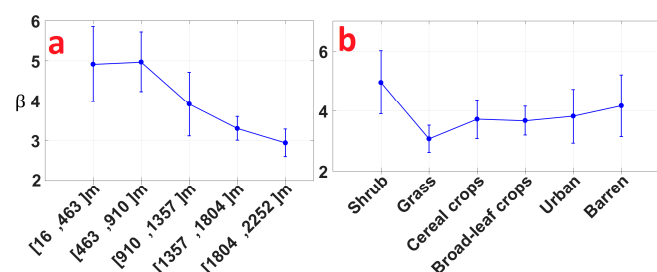


Figure 5. Mean and standard deviation of β values for weather stations with different (a) DEM classes, and (b) land covers.

5.1. Estimation of the Air DTC Model Based on LST DTC Parameters

In the next step, the dataset was divided into two parts. Seventy percent of the dataset for both air temperature and LST were used for estimating the regression coefficients at each equation and

the rest were used for testing the estimated air DTC model. According to Equations (11)–(14), the air DTC model was estimated based on the LST DTC model. After estimation of the regression models' coefficients and the air DTC model parameters, the air DTC model at each weather station for the whole time series was constructed. To present the result of air temperature modeling, six sample DTC models in the study area are shown in Figure 6. Ahvaz, Arak, Hamedan, Omidiyeh, Baft, and Shahrekurd are the sample stations shown in Figure 6 on 221st day of 2016 (8 August). The turquoise blue line shows the LST DTC model, the green line is the air DTC model constructed from observation, and black line demonstrates the estimated air DTC model from regression equations. Blue dots show the LST observations, red dots are air temperature observations, and black dots are estimated air temperatures from regression equations (Equations (11)–(14)) at observation times of the weather stations. According to Figure 6, and the following explanations, the results show appropriate correspondence among the estimated air DTC models (from the regression), constructed air DTC models from observations, and air temperature observations. In some parts of DTC models, some small shifts exist which show the error in LST and air DTC modeling. These errors can also be attributed to environmental variables. To compare the values of parameters, the free DTC parameters of LST were subtracted from their counterparts in air DTC model and their mean was calculated. Figure 7 shows the mean differences of parameters for the whole time period in the study area. In Figure 7a the $T_0 - T_{min}$ was between $-4.2\text{ }^{\circ}\text{C}$ to $+4.2\text{ }^{\circ}\text{C}$. In South West of Iran the T_0 values of LST were higher than T_{min} values in air DTC model.

Figure 7b shows that $T_{\max_{LST}} - T_{\max_{air}}$ ($T_{\max_{LST}} = T_0 + A$) was between $4\text{ }^{\circ}\text{C}$ and $18\text{ }^{\circ}\text{C}$. In Figure 7c the $t_{m_{LST}} - t_{m_{air}}$ varied between -3.9 and -2.5 h . This shows that in all weather stations t_m of air DTC models happened after t_m in LST DTC models. In other words, air reached maximum daily temperature with delay compared to LST. In Figure 7d $t_{s_{LST}} - t_{s_{air}}$ were between -5.9 and -3.7 h . In North West of Iran, these differences were lower and in bare lands were higher.

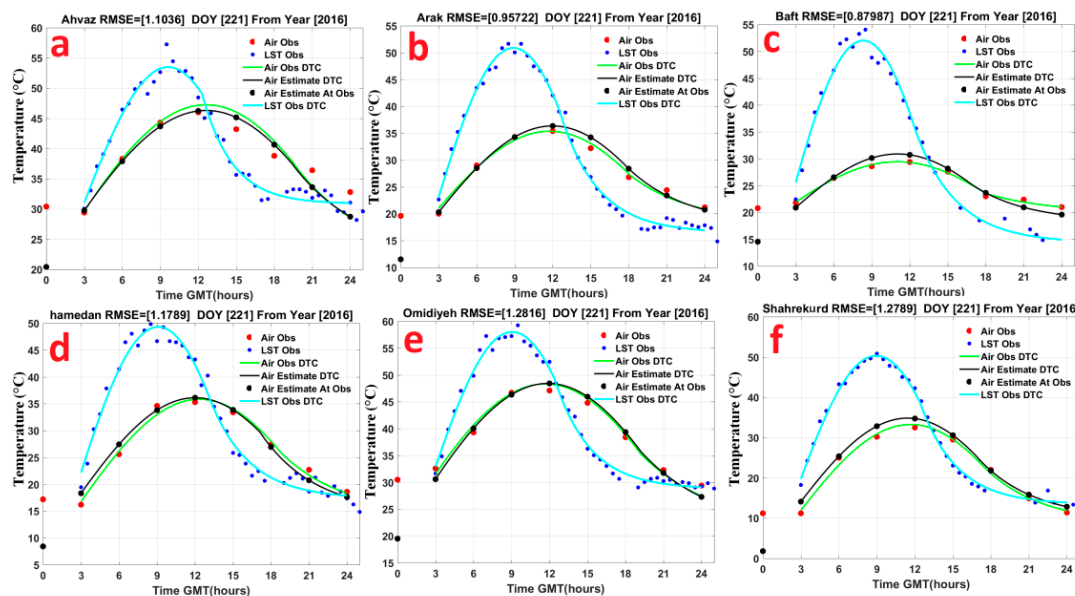


Figure 6. Comparisons of air temperature and LST DTCs. Turquoise blue line shows the LST DTC model. Green line is air DTC model extracted from the observations (red dots). The black line is the air DTC model constructed from the regression approach with concurrent weather station observations (black dots); (a) Ahvaz, (b) Arak, (c) Baft, (d) Hamedan, (e) Omidiyeh, and (f) Shahrekurd weather stations.

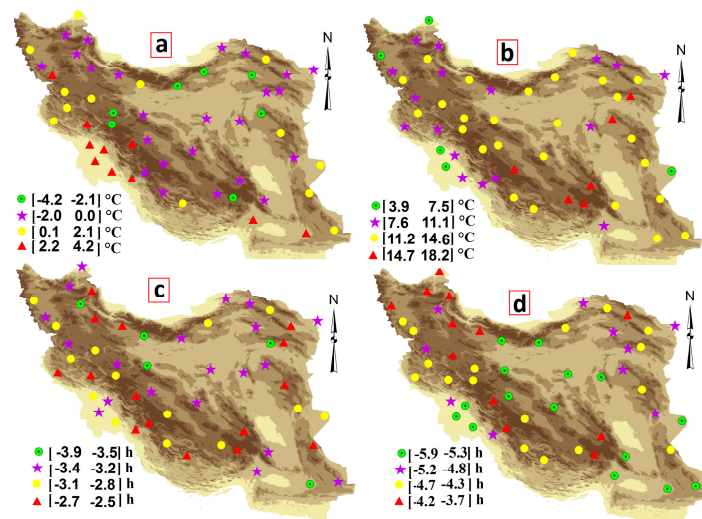


Figure 7. Differences of LST and air DTC parameters in the study area. (a) $T_0 - T_{min}$, (b) $T_{maxLST} - T_{maxair}$, and (c) $t_{mLST} - t_{mair}$ (d) $t_{sLST} - t_{sair}$.

5.2. Accuracy of the Air DTC Model from Regressions

The accuracy of all the constructed air DTC models was evaluated by weather station three-hour observations (the remained 30% of the dataset). The error, MAE and RMSE for each weather station was calculated from subtracting weather station air temperature values from their concurrent values in the estimated air DTC model. Error bars that contain the mean and RMSE for the three-hour sample time are shown in Figure 8a. The mean error ranges varies between $[-0.29, 0.6]$ °C and RMSE is also was between $[2, 2.11]$ °C (Figure 8a). To analyze the accuracy of constructed air DTC models for whole diurnal stages, the MAEs and RMSEs were calculated for each daily modeling. The MAE values varied between 0.1 to 4 °C. The RMSE range was between 0.1 and 3.3 °C (Figure 8b,c). The mean of the MAEs was 1.6 °C. Most of the RMSEs were almost between 1 and 2.4 °C (Figure 8b,c). Considering the different climate regimes in the study area, the inherent errors in modeling between LST and air temperature resulted from environmental variables; both histograms show acceptable results of air DTC modeling from the regression analysis. Figure 9 depicts mean error and RMSEs of DTC modeling for different elevation and land cover classes from 3 to 21 GMT sample time. Figure 9a shows the error bar of air DTC modeling at five elevation classes. Low elevation classes (16 to 463 m) with a -2.29 °C mean error and 2.32 °C RMSE depicting more separation from others and its discrepancies were the utmost at 18:00 GMT; high elevation classes (1804 to 2252 m) with -0.92 °C mean error and the 2.09 °C RMSE had the lowest values at 18:00 GMT time.

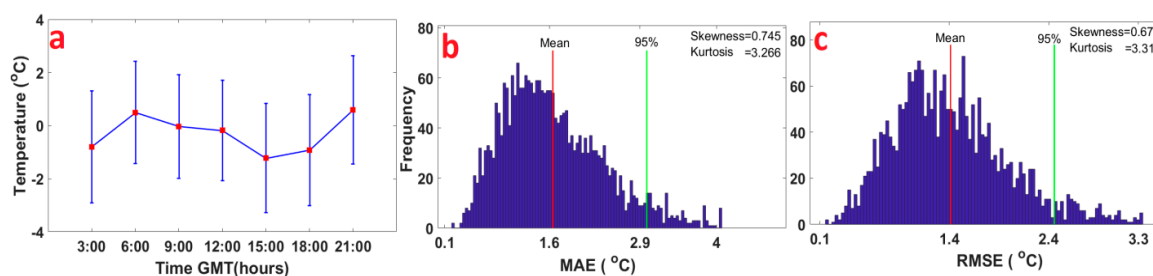


Figure 8. Statistics for differences between modeled and observation air temperatures for all stations. (a) error bars of sample time, (b) histogram of MAEs, and (c) histogram of RMSEs for all 54 stations and seven sample times.

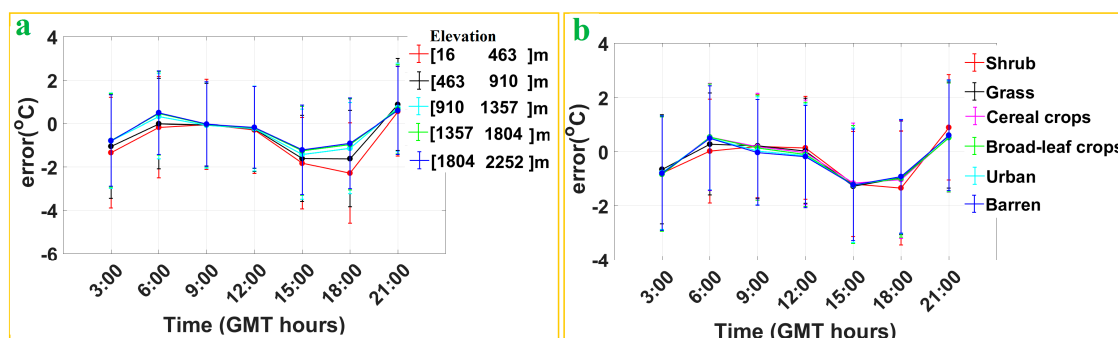


Figure 9. Mean and RMSEs of model errors in weather stations for different land covers and elevation (DEM) classes at different times. (a) Elevation class errors, and (b) land cover type errors.

The error bar of the model in shrub land cover at 18:00 GMT with -1.34°C mean error and 2.10°C RMSE is more separated from others.

6. Discussion

A large number of variables affect air temperature like topography, vegetation, soil type, soil moisture, aerosol, distance to coast, wind, solar geometry, incoming solar radiation, long-wave upwelling radiation, long-wave downwelling radiation, sensible heat flux, latent heat flux, and ground heat flux. In fact, the complex interactions of the mentioned variables at the micro and macro scales influence air temperature. The density and spatial distribution of weather stations are also two influential factors for modeling air temperature. LST is affected by these variables and it can be directly related to air temperature in complex environments. Results showed the possibility of modeling air temperature in a continuous temporal space by LST DTC models. Linear regression was used to model air DTC free parameter's based on LST DTC free parameters. β was considered as a constant parameter and estimated experimentally; its range was between 2.4 and 8 and the spatial variations of this parameter can be attributed to environmental condition. This parameters control the period of cosine term and its effect is until starting attenuation time (t_s). The regression equations were used for estimating the air DTC parameters. Based on these parameters, the air DTC models at each station were constructed. The comparison of DTC parameters of LST and air temperature showed T_0 and T_{\min} had difference range between -4.2°C and $+4.2^{\circ}\text{C}$ which varied spatially. The time of maximum temperature in air and LST varied between -3.9 to -2.5 h; this showed that the delay time of the diurnal maximum air temperature is in contrast with the maximum diurnal LST. t_s differences were between -5.9 to -3.7 h, which is related to the existence of the mentioned delay which existed between t_m in both DTCs. The estimated constructed air DTC models were evaluated with weather observations from 03:00 to 21:00 GMT three-hourly by MAE and RMSE. Elevation and land cover classes have the same pattern of model error bars in sine form over the sample time. Low elevation and shrub land cover classes were more separated from other categories at six and 18 h. The range of 95% of MAEs for all stations varied between 0.8 to 2.9°C and for RMSEs was between 0.1 and 2.4°C . The results showed that although the study area had many complexities forced by topography, weather systems, and diverse land covers the modeling accuracy of proposed method was acceptable. Although the error is much larger than the variation caused by land cover type and time of day; the authors think the only way to reduce that error is with more station data.

7. Conclusions

The results showed that the INSAT-3D LST data could be used to estimate air temperature continuously by using direct DTC models parameters. The evaluations of result showed an acceptable error between observations and the model with 95% of MAEs in the range $[0.1, 2.9]^{\circ}\text{C}$ and RMSE in the range $[0.1, 2.4]^{\circ}\text{C}$; it can be concluded that the estimated coefficients from regression analysis

could model the influence of environmental variables and the discrepancies between air temperature and LST with acceptable accuracy. Therefore, it is possible to estimate air temperature by LST in day and night under clear sky conditions for different land covers and elevation classes in the study area. Additionally, the DTC parameters of LST and air temperature were compared with each other in all studied stations. Although different elevation and land cover classes have some small separation from each other, their total behavior were the same and similar to the sine form, which showed the efficiency of the proposed model over diverse elevation and land cover classes. Further research is required to examine different climate conditions and land covers to test the applicability of this method in other areas and it is essential that more research be conducted to provide explorations about the physical basis of β parameters and its relation to environmental factors.

Acknowledgments: The authors specially thank the Land Processes Distributed Active Archive Center (LP DAAC) for providing the MODIS LST, ASTER GDEM as a product of METI and NASA, land cover products, and the Meteorological and Oceanographic Satellite Data Archival Centre (MOSDAC) for giving access to Imager LST products. The authors actually thank Iranian National Science Foundation and Iranian National Space Administration for their strong supports this research.

Author Contributions: Gholamnia conducted the analysis. Seyed Kazem Alavipanah managed the research. Darvishi provided technical support. Hamzeh provided great help in writing the manuscript. Kiavarz helped in organizing the materials.

Conflicts of Interest: The authors declare no conflict of interest.

References

- Parton, W.J.; Logan, J.A. A model for diurnal variation in soil and air temperature. *Agric. Meteorol.* **1981**, *23*, 205–216. [[CrossRef](#)]
- Gázquez, F.; Calaforra, J.M.; Fernández-Cortés, Á. Flash flood events recorded by air temperature changes in caves: A case study in Covadura Cave (Se Spain). *J. Hydrol.* **2016**, *541*, 136–145. [[CrossRef](#)]
- Bunker, A.; Wildenhain, J.; Vandenbergh, A.; Henschke, N.; Rocklöv, J.; Hajat, S.; Sauerborn, R. Effects of air temperature on climate-sensitive mortality and morbidity outcomes in the elderly; a systematic review and meta-analysis of epidemiological evidence. *EBioMedicine* **2016**, *6*, 258–268. [[CrossRef](#)] [[PubMed](#)]
- Deser, C.; Terray, L.; Phillips, A.S. Forced and internal components of winter air temperature trends over North America during the past 50 years: Mechanisms and implications. *J. Clim.* **2016**, *29*, 2237–2258. [[CrossRef](#)]
- Slini, T.; Papakostas, K. 30 years air temperature data analysis in Athens and Thessaloniki, Greece. In *Energy, Transportation and Global Warming*; Springer: Berlin, Germany, 2016; pp. 21–33.
- Sun, Y.-J.; Wang, J.-F.; Zhang, R.-H.; Gillies, R.; Xue, Y.; Bo, Y.-C. Air temperature retrieval from remote sensing data based on thermodynamics. *Theor. Appl. Climatol.* **2005**, *80*, 37–48. [[CrossRef](#)]
- Prince, S.D.; Goetz, S.J.; Dubayah, R.; Czajkowski, K.; Thawley, M. Inference of surface and air temperature, atmospheric precipitable water and vapor pressure deficit using advanced very high-resolution radiometer satellite observations: Comparison with field observations. *J. Hydrol.* **1998**, *212*, 230–249. [[CrossRef](#)]
- Zakšek, K.; Schroedter-Homscheidt, M. Parameterization of air temperature in high temporal and spatial resolution from a combination of the SEVIRI and MODIS instruments. *ISPRS J. Photogramm. Remote Sens.* **2009**, *64*, 414–421. [[CrossRef](#)]
- Prihodko, L.; Goward, S.N. Estimation of air temperature from remotely sensed surface observations. *Remote Sens. Environ.* **1997**, *60*, 335–346. [[CrossRef](#)]
- Stisen, S.; Sandholt, I.; Nørgaard, A.; Fensholt, R.; Eklundh, L. Estimation of diurnal air temperature using MSG SEVIRI data in West Africa. *Remote Sens. Environ.* **2007**, *110*, 262–274. [[CrossRef](#)]
- Nieto, H.; Sandholt, I.; Aguado, I.; Chuvieco, E.; Stisen, S. Air temperature estimation with MSG-SEVIRI data: Calibration and validation of the TVX algorithm for the IBERIAN PENINSULA. *Remote Sens. Environ.* **2011**, *115*, 107–116. [[CrossRef](#)]
- Zhu, W.; Lü, A.; Jia, S. Estimation of daily maximum and minimum air temperature using MODIS land surface temperature products. *Remote Sens. Environ.* **2013**, *130*, 62–73. [[CrossRef](#)]
- Goetz, S.; Prince, S.D. Modelling terrestrial carbon exchange and storage: Evidence and implications of functional convergence in light-use efficiency. *Adv. Ecol. Res.* **1999**, *28*, 57–92.

14. Florio, E.; Lele, S.; Chi Chang, Y.; Sterner, R.; Glass, G. Integrating AVHRR satellite data and NOAA ground observations to predict surface air temperature: A statistical approach. *Int. J. Remote Sens.* **2004**, *25*, 2979–2994. [[CrossRef](#)]
15. Sandholt, I.; Rasmussen, K.; Andersen, J. A simple interpretation of the surface temperature/vegetation index space for assessment of surface moisture status. *Remote Sens. Environ.* **2002**, *79*, 213–224. [[CrossRef](#)]
16. Mostovoy, G.V.; King, R.L.; Reddy, K.R.; Kakani, V.G.; Filippova, M.G. Statistical estimation of daily maximum and minimum air temperatures from MODIS LST data over the state of MISSISSIPPI. *Glsci. Remote Sens.* **2006**, *43*, 78–110. [[CrossRef](#)]
17. Vancutsem, C.; Ceccato, P.; Dinku, T.; Connor, S.J. Evaluation of modis land surface temperature data to estimate air temperature in different ecosystems over Africa. *Remote Sens. Environ.* **2010**, *114*, 449–465. [[CrossRef](#)]
18. Benali, A.; Carvalho, A.; Nunes, J.; Carvalhais, N.; Santos, A. Estimating air surface temperature in Portugal using MODIS LST data. *Remote Sens. Environ.* **2012**, *124*, 108–121. [[CrossRef](#)]
19. Zhu, W.; Lü, A.; Jia, S.; Yan, J.; Mahmood, R. Retrievals of all-weather daytime air temperature from modis products. *Remote Sens. Environ.* **2017**, *189*, 152–163. [[CrossRef](#)]
20. Cresswell, M.; Morse, A.; Thomson, M.; Connor, S. Estimating surface air temperatures, from Meteosat land surface temperatures, using an empirical solar zenith angle model. *Int. J. Remote Sens.* **1999**, *20*, 1125–1132. [[CrossRef](#)]
21. Emamifar, S.; Rahimikhoob, A.; Noroozi, A.A. Daily mean air temperature estimation from MODIS land surface temperature products based on M5 model tree. *Int. J. Climatol.* **2013**, *33*, 3174–3181. [[CrossRef](#)]
22. Fu, G.; Shen, Z.; Zhang, X.; Shi, P.; Zhang, Y.; Wu, J. Estimating air temperature of an alpine meadow on the northern tibetan plateau using MODIS land surface temperature. *Acta Ecol. Sin.* **2011**, *31*, 8–13. [[CrossRef](#)]
23. Jang, J.-D.; Viau, A.; Anctil, F. Neural network estimation of air temperatures from AVHRR data. *Int. J. Remote Sens.* **2004**, *25*, 4541–4554. [[CrossRef](#)]
24. Kim, D.-Y.; Han, K.-S. Remotely sensed retrieval of midday air temperature considering atmospheric and surface moisture conditions. *Int. J. Remote Sens.* **2013**, *34*, 247–263. [[CrossRef](#)]
25. Lin, S.; Moore, N.J.; Messina, J.P.; DeVisser, M.H.; Wu, J. Evaluation of estimating daily maximum and minimum air temperature with modis data in east africa. *Int. J. Appl. Earth Obs. Geoinf.* **2012**, *18*, 128–140. [[CrossRef](#)]
26. Moser, G.; De Martino, M.; Serpico, S.B. Estimation of air surface temperature from remote sensing images and pixelwise modeling of the estimation uncertainty through support vector machines. *IEEE J. Sel. Top. Appl. Earth Observ. Remote Sens.* **2015**, *8*, 332–349. [[CrossRef](#)]
27. Vogt, J.V.; Viau, A.A.; Paquet, F. Mapping regional air temperature fields using satellite-derived surface skin temperatures. *Int. J. Climatol.* **1997**, *17*, 1559–1579. [[CrossRef](#)]
28. Xu, Y.; Qin, Z.; Shen, Y. Study on the estimation of near-surface air temperature from MODIS data by statistical methods. *Int. J. Remote Sens.* **2012**, *33*, 7629–7643. [[CrossRef](#)]
29. Yan, H.; Zhang, J.; Hou, Y.; He, Y. Estimation of air temperature from MODIS data in east China. *Int. J. Remote Sens.* **2009**, *30*, 6261–6275. [[CrossRef](#)]
30. Zhang, W.; Huang, Y.; Yu, Y.; Sun, W. Empirical models for estimating daily maximum, minimum and mean air temperatures with MODIS land surface temperatures. *Int. J. Remote Sens.* **2011**, *32*, 9415–9440. [[CrossRef](#)]
31. Xu, Y.; Knudby, A.; Ho, H.C. Estimating daily maximum air temperature from MODIS in British Columbia, Canada. *Int. J. Remote Sens.* **2014**, *35*, 8108–8121. [[CrossRef](#)]
32. Duan, S.-B.; Li, Z.-L.; Wang, N.; Wu, H.; Tang, B.-H. Evaluation of six land-surface diurnal temperature cycle models using clear-sky in situ and satellite data. *Remote Sens. Environ.* **2012**, *124*, 15–25. [[CrossRef](#)]
33. Jin, M.; Dickinson, R.E. Interpolation of surface radiative temperature measured from polar orbiting satellites to a diurnal cycle: 1. without clouds. *J. Geophys. Res. Atmos.* **1999**, *104*, 2105–2116. [[CrossRef](#)]
34. Sun, D.; Pinker, R.T.; Kafatos, M. Diurnal temperature range over the United States: A satellite view. *Geophys. Res. Lett.* **2006**, *33*. [[CrossRef](#)]
35. Alavipanah, S.K.; Weng, Q.; Gholamnia, M.; Khandan, R. An analysis of the discrepancies between MODIS and INSAT-3D LSTs in high temperatures. *Remote Sens.* **2017**, *9*, 347. [[CrossRef](#)]
36. Inamdar, A.K.; French, A.; Hook, S.; Vaughan, G.; Luckett, W. Land surface temperature retrieval at high spatial and temporal resolutions over the southwestern United States. *J. Geophys. Res. Atmos.* **2008**, *113*. [[CrossRef](#)]

37. EPSA. *INSAT-3D Algorithm Theoretical Basis Document*; Space Applications Centre, Government of India: Ahmedabad, India, 2015.
38. Duffie, J.A.; Beckman, W.A. *Solar Engineering of Thermal Processes*; Wiley: New York, NY, USA, 1980.
39. ELAGIB, N.A.; ALVI, S.H.; MANSELL, M.G. Day-length and extraterrestrial radiation for Sudan: A comparative study. *Int. Sol. Energy* **1999**, *20*, 93–109. [[CrossRef](#)]
40. Göttsche, F.-M.; Olesen, F.S. Modelling of diurnal cycles of brightness temperature extracted from Meteosat data. *Remote Sens. Environ.* **2001**, *76*, 337–348. [[CrossRef](#)]
41. Schädlich, S.; Göttsche, F.; Olesen, F.-S. Influence of land surface parameters and atmosphere on METEOSAT brightness temperatures and generation of land surface temperature maps by temporally and spatially interpolating atmospheric correction. *Remote Sens. Environ.* **2001**, *75*, 39–46. [[CrossRef](#)]



© 2017 by the authors. Licensee MDPI, Basel, Switzerland. This article is an open access article distributed under the terms and conditions of the Creative Commons Attribution (CC BY) license (<http://creativecommons.org/licenses/by/4.0/>).